Journal of King Saud University – Science (2018) 30, 229–249

King Saud University
Journal of King Saud University – Science
www.ksu.edu.sa
www.sciencedirect.com

Structural and vibrational characterization of anhydrous and dihydrated species of trehalose based on the FTIR and FTRaman spectra and DFT calculations

María Jimena Márquez [a], Davide Romani [b], Sonia Beatriz Díaz [c], Silvia Antonia Brandán [a,*]

[a] Cátedra de Química General, Instituto de Química Inorgánica, Facultad de Bioquímica, Química y Farmacia, Universidad Nacional de Tucumán, Ayacucho 471, 4000 San Miguel de Tucumán, Tucumán, Argentina
[b] SST, Servicio sanitario della Toscana, Azienda USL 9 di Grosseto, Via Cimabue, 109, 58100 Grosseto, Italy
[c] Cátedra de Fisicoquímica, Instituto de Química Física, Facultad de Bioquímica, Química y Farmacia, Universidad Nacional de Tucumán, San Lorenzo 456, 4000 San Miguel de Tucumán, Tucumán, Argentina

Received 26 October 2016; accepted 18 January 2017
Available online 25 January 2017

KEYWORDS

Trehalose;
Molecular structure;
Vibrational spectra;
DFT calculations;
Force field

Abstract In this study, three anhydrous species of trehalose and their dihydrated form were studied using the Fourier Transform Infrared (FTIR) and Raman spectroscopy combined with theoretical calculations derived from the theory of the functional of the density (DFT). Here, the structural and vibrational properties were predicted using the hybrid B3LYP/6-31G* method. The complete vibrational assignments were performed using the scaled mechanical force fields (SQMFF) methodology and their internal normal coordinates. The natural bond orbital (NBO) and atoms in molecules (AIM) calculations predicted high stabilities for the dihydrated species in gas and aqueous solution phases. The little variation observed in the dipole moment for the dihydrated species in solution could be related to a small perturbation of water hydration shell and short hydrogen bonds, as revealed by NBO and AIM studies. The lower volume expansion, low solvation energy and the higher nucleophilicity index observed for trehalose species in solution, in relation to maltose and sucrose could probably explain that different water molecules are around of trehalose/water mixtures generating higher "rigidity" in trehalose, as was experimentally reported in the literature. On the other hand, the low $f(\nu O–H)_{H2O}$ force constant value for trehalose, as compared with maltose and lactose could justify the very fragile character from the trehalose/water system to

* Corresponding author. Fax: +54 381 4248169.
E-mail address: sbrandan@fbqf.unt.edu.ar (S.A. Brandán).
Peer review under responsibility of King Saud University.

Production and hosting by Elsevier

http://dx.doi.org/10.1016/j.jksus.2017.01.009

the temperature and concentration changes, as was experimentally observed from viscosity and Raman scattering studies.

1. Introduction

The structural and vibrational properties of some important disaccharides were recently reported by our investigation group (Brizuela et al., 2012a,b, 2014; Márquez et al., 2015a,b; Iramain et al., 2016). In this work, those properties for anhydrous and dihydrated species derived from trehalose were also studied because they are important due to the variety of their uses and applications (Schebor et al., 2010; Shibata and Nagashima, 2016; Yano et al., 2015; Kawashima and Goto, 2011; Connolly et al., 2010; Magazù et al., 2010a,b; Calabrò and Magazù, 2012; Siddhanta et al., 2015; Takahashi et al., 2006; Govindarajan et al., 2006; Belton and Gil, 1994) and, also, because its sugar is a nonreducing disaccharide of glucose that modifies the physical properties of membrane phospholipids in the dry state and, as a consequence, the notable stability of membranes in anhydrobiotic organisms can be explained, as was reported by Crowe and Crowe (1984). There are many studies related to the use of the vibrational spectroscopy on trehalose species, for instance, recent studies on the bioprotective effect of trehalose on human hemoglobin (Connolly et al., 2010; Calabrò and Magazù, 2012), on the interaction of trehalose with Hen egg white lysozyme (Belton and Gil, 1994) and, also on the low-frequency vibrations below 200 cm^{-1} of crystalline αα-trehalose dihydrate (Takahashi et al., 2006) using far-infrared spectroscopy but, so far, the infrared and Raman spectra of trehalose were not completely assigned. From a structural point of view, there are three known trehalose species anhydrous, one of them, the αα-trehalose isomer (α-D-glucopyranosyl α-D-glucopyranoside) is found in natural form while the other two αβ-trehalose and ββ-trehalose isomers were synthesized. On the other hand, the crystal structure of trehalose dihydrate in the solid phase was already reported in an independent form by Taga et al. (1972) and Brown et al. (1972). Hence, we have studied the structural and vibrational properties of those three trehalose anhydrous species and their αα-dihydrated form which were compared first among them and, later with the properties reported for similar sugars (Brizuela et al., 2012a,b, 2014; Márquez et al., 2015a,b; Iramain et al., 2016). Hence, the aim of this work is to perform a combined study using theoretical calculations based on the density functional theory (DFT) and the experimental infrared and Raman spectra for the αα-trehalose dihydrated in the solid state. With this purpose, the structures of those four trehalose species were optimized using the B3LYP/6-31G* level (Becke, 1993; Lee et al., 1988) in gas and aqueous solution phases and, later the atomic charges, molecular electrostatic potentials, stabilization energies, bond orders, frequencies and topological properties were calculated at the same level of theory. On the other hand, the force fields for those structures in both media were also calculated using the scaled quantum mechanical force field (SQMFF) methodology (Rauhut and Pulay, 1995a,b) accomplished with the corresponding normal internal coordinates in order to perform the vibrational analyses using the Molvib program (Sundius, 2002). In addition, the reactivities and behaviors of those four trehalose species in the different media were also predicted using the corresponding frontier orbitals and some known descriptors reported in the literature (Parr and Pearson, 1983; Brédas, 2014; Márquez and Brandán, 2014; Cataldo et al., 2014; Romani and Brandán, 2015a; Romani et al., 2015b; Márquez et al., 2015a,b). Here, the structural and vibrational properties for the trehalose species in aqueous solution were evaluated and analyzed in accordance with those publications reported for trehalose by different authors (Pagnotta et al., 2008; Varga et al., 2008; Magazù et al., 2007; Olsson et al., 2016; Magazù et al., 1998, 1999, 2010a,b, 2011; Ballone et al., 2000; Branca et al., 1999, 2001, 2002; Bonanno et al., 1998).

2. Experimental methods

A commercial sample of anhydrous αα-trehalose dihydrate in pure solid state was used to prepare KBr pellets. The infrared spectrum was recorded on a Fourier Transform Infrared (FT-IR) Perkin Elmer spectrophotometer in the wavenumbers ranging from 4000 to 400 cm^{-1} provided with a Globar source and DGTS detector. The Raman spectra of the compound in solid state was recorded between 4000 and 10 cm^{-1} with a Bruker RF100/S spectrometer equipped with a Nd:YAG laser (excitation line of 1064 nm, 800 mW of laser power) and a Ge detector cooled at liquid nitrogen temperature. The IR and Raman spectra were recorded with 200 scans and a resolution of 1 cm^{-1}.

3. Computational details

The initial structures of those four species of trehalose were modeled with the *GaussView* program (Nielsen and Holder, 2008) and, then, they were optimized in the gas phase and in aqueous solution using the hybrid B3LYP/6-31G* method and the Gaussian 09 program (Frisch et al., 2009). In this study, two different αα-dihydrated species were considered and, also, the dimeric species corresponding to the most stable dihydrated species in accordance to the experimental structures reported (Taga et al., 1972; Brown et al., 1972). The calculations for all the species in aqueous solution were performed using the self consistent reaction field (SCRF) method together with the polarized continuum (PCM) and solvation (SD) models (Tomasi and Persico, 1994; Miertus et al., 1998; Marenich et al., 2009). Both models were used to compute the solvation energies while the changes in the volume of these species in solution in relation to the values in gas phase were estimated with the Moldraw program (Ugliengo, 1998). The three anhydrous species can be seen in Fig. 1 while the αα-dihydrated species is shown in Fig. 2. The dimeric structure for the most stable αα-dihydrated structure is presented in

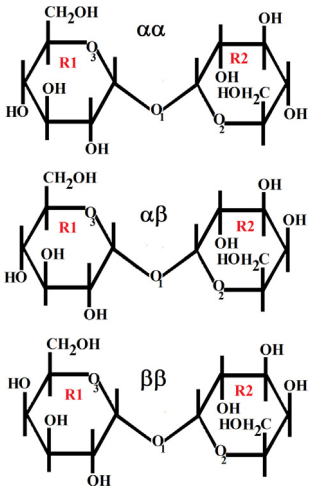

Figure 1 Theoretical anhydrous structures of αα-, αβ and ββ-trehalose indicating the atoms labeling for the O atoms corresponding to the glycosidic and glucopyranose rings.

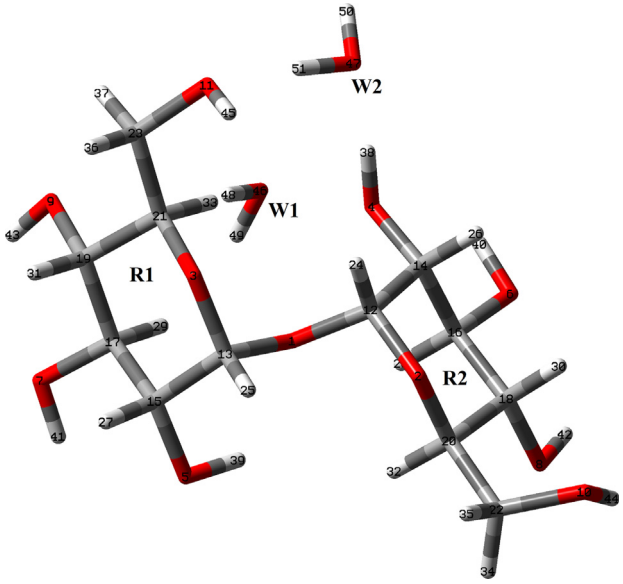

Figure 2 Theoretical structure of αα-dihydrated trehalose species together with the atoms labeling. The water molecules are indicated by W letters.

Fig. 3. On the other hand, in Fig. S1 the detailed theoretical structures of αα-, αβ- and ββ-trehalose anhydrous species showing the identification of the R1 and R2 glucopyranose rings are presented. Here, two atomic charges types were studied, the Merz–Kollman (MK) and the natural population atomic (NPA) which were computed with the natural bond orbital (NBO) and Gaussian programs (Besler et al., 1990; Glendening et al., 1996). On the other hand, the molecular electrostatic potential values for all the species were calculated using the MK charges while the bond order and the stabilization energy values for all those species were obtained from the NBO calculations at the same level of theory. The intermolecular interactions were also analyzed by means the topological properties which were calculated using the AIM2000 program (Biegler-Köning et al., 2001). In addition, the reactivities of the anhydrous and dihydrated species in the different media were predicted using the corresponding frontier orbitals (Parr and Pearson, 1983; Brédas, 2014) while the chemical potential (μ), electronegativity (χ), global hardness (η), global softness (S) and global electrophilicity index (ω) descriptors were employed in order to predict their behaviors at the same level of theory (Márquez and Brandán, 2014; Cataldo et al., 2014; Romani and Brandán, 2015a; Romani et al., 2015b; Márquez et al., 2015a,b). Here, it is necessary to clarify that the equations corresponding to these descriptors were presented in the Supporting material because they are widely known in the literature. On the other hand, the internal coordinates used in the determination of the force fields for the anhydrous and dihydrated species were those similar to the ones reported for other sugars (Brizuela et al., 2012a; 2014) and, for this reason, they were not presented here. The force fields obtained for all the species with the SQMFF procedure (Rauhut and Pulay, 1995a,b) and the Molvib program (Sundius, 2002) in Cartesian coordinates were later transformed to internal coordinates. Here, we have used the potential energy distribution components (PED) $\geqslant$ 10% in order to perform the complete vibrational assignments of those anhydrous and dihydrated species while the assignments for the dimeric species were performed with the aid of the *GaussView* program (Nielsen and Holder, 2008).

4. Results and discussion

4.1. Structural analysis

Table 1 shows the calculated total and relative energies, dipole moments and populations for all the studied trehalose species in gas and aqueous solution phases. Here, we have considered two different structures for the αα-trehalose anhydrous and dihydrated species, named C1 and C2 in order to find the most stable species, as observed in Table 1. The results clearly show that the αβ anhydrous and the C1αα- dihydrated species are the most stables and, hence, the higher populations are found for the αβ- anhydrous species in gas phase with a value of 60% while in solution the value decreases up to 35.33%, then, the population of the ββ species increases drastically in this medium from 0.16% in the gas phase up to 46.30%. In relation to the dipole moment values, in gas phase the three anhydrous species show similar values while their values notably change in solution observing a particular decrease in the value for the ββ species. This notable reduction in the dipole moment value for the anhydrous ββ species could probably be related to their major volume expansion in solution and to their higher solvation energy value, as will see later. The dipole moment values for the two dihydrated species also increase in solution presenting the most stable species the higher value in gas phase but the lower value in solution, in relation to the C2 species. Here, the few variations observed in the dipole moments for the dihydrated species in solution could be related to a small perturbation of water hydration shell and short hydrogen bonds between trehalose oxygens and water hydrogens, as reported by Pagnotta et al. (2008). The αα dimeric species present an energy value of −2901.5588 Hartrees in gas phase with a dipole moment value of 6.05 D. This way, this dimeric species show a higher stability as compared to two units of αα

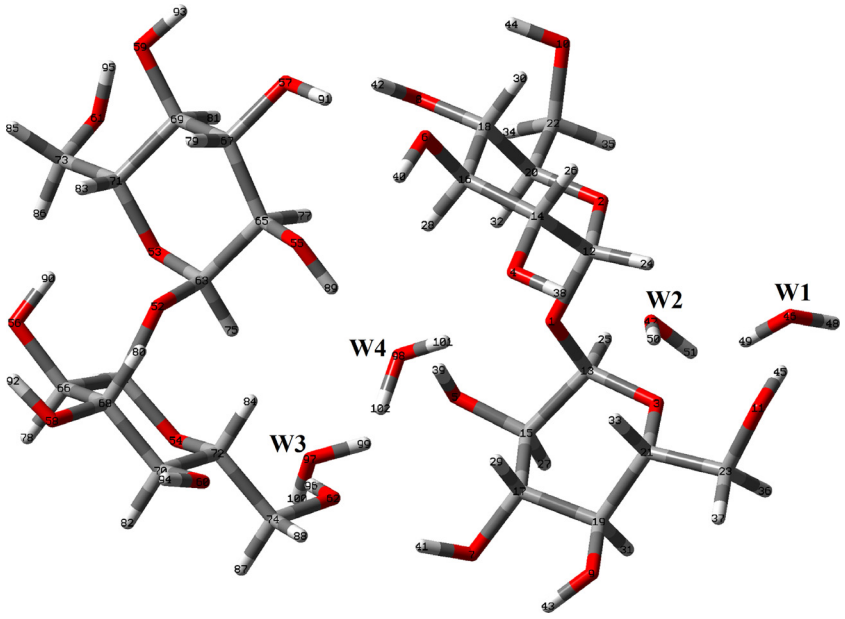

Figure 3 Theoretical dimeric structure of αα-dihydrated trehalose species together with the atoms labeling.

Table 1 Calculated total (*E*) and relative energies (Δ*E*), dipole moments and populations (%) for the trehalose species in gas and aqueous solution phases.

B3LYP/6-31G*								
	GAS				PCM			
Species	E (hartree)	μ (D)	ΔE kJ/mol	Population %	E (hartree)	μ (D)	ΔE kJ/mol	Population %
Anhydrous								
C1αα	−1297.8870	2.80	1.05	39.33	−1297.9415	4.36	0.52	18.37
αβ	−1297.8874	2.84	0.00	60.51	−1297.9417	3.35	0.00	35.33
ββ	−1297.8818	2.72	14.69	0.16	−1297.9412	0.81	1.31	46.30
C2αα	−1297.8733	3.25	36.98	0.00	−1297.9372	3.70	11.80	0.00
Dihydrated								
C1αα	−1450.7569	3.70	0.00	100	−1450.8214	4.54	0.00	100
C2αα	−1450.7376	3.44	50.63	0.00	−1450.8096	6.05	30.95	0.00

dihydrated species, it is $2 \times -1450.7569 = -2901.5138$ Hartrees.

A comparison of the calculated geometrical parameters for the anhydrous and dihydrated species of trehalose in gas phase with those corresponding experimental ones for the dihydrated species (Taga et al., 1972 and Brown et al., 1972) by means of the root-mean-square deviation (RMSD) values can be seen in Table 2. The RMSD values show a very good agreement for the bond lengths and angles of all the species and, especially, in the dihedral angles of the dihydrated species with a difference only of 7.4° while for the anhydrous species the RMSD values vary between 65.5 and 38.1°, as expected because the compared experimental species is also dihydrated. Note that the higher differences among the structures are observed in the dihedral C18–C20–C22–O10 angles where only the dihydrated species has a value close to the experimental one, as explained before. In general, the optimized parameters are underestimated by the B3LYP/6-31G* calculations, in reference to the experimental values and, only some calculated distances are approximately similar in all the species such as those C–C bonds belonging to the ring R1. Probably, this observation can be explained because the α-D-glucopyranosyl R1 ring remains practically constant in the αα, αβ and ββ species including the dihydrated one while the other α-D-glucopyranoside ring R2 change in the αβ and ββ species. For this reason, both αα anhydrous and dihydrated species have practically similar bond lengths values with exception of the C13–O1, C20–C22, C21–C23, C14–O4 and C18–O8 bonds which show slightly variations in the values, as indicated in Table 2.

4.2. Volume variations and solvation energies

The molecular volume variations (Ugliengo, 1998) observed in the anhydrous and dihydrated species in solution, in reference to the values in the gas phase and, the calculated solvation energies at the B3LYP/6-31G* calculations level using the polarized continuum (PCM) and solvation (SD) models

Table 2 Comparison of calculated geometrical parameters for the anhydrous and dihydrated species of trehalose in gas phase with the corresponding experimental ones.

B3LYP/6-31G*[a]					
Parameter	Anhydrous			Dihydrated	
	α-α-trehalose	α-β-trehalose	β-β-trehalose	α-α-trehalose	Exp[b] α-α-trehalose
Bond lengths (*Å*)					
C12–O1	1.431	1.434	1.437	1.431	1.417 (5)
C13–O1	1.433	1.431	1.427	1.406	1.421 (5)
C12–O2	1.405	1.401	1.400	1.408	1.423 (5)
C20–O2	1.446	1.446	1.446	1.442	1.437 (5)
C13–O3	1.399	1.401	1.408	1.425	1.407 (5)
C21–O3	1.442	1.442	1.449	1.455	1.424 (6)
C14–C12	1.534	1.530	1.530	1.542	1.514 (6)
C14–C16	1.530	1.531	1.531	1.526	1.523 (6)
C16–C18	1.525	1.532	1.533	1.518	1.526 (6)
C18–C20	1.529	1.531	1.529	1.529	1.533 (6)
C13–C15	1.534	1.534	1.534	1.534	1.531 (6)
C15–C17	1.530	1.529	1.534	1.531	1.513 (6)
C17–C19	1.526	1.525	1.539	1.525	1.514 (6)
C19–C21	1.532	1.533	1.535	1.532	1.526 (6)
C20–C22	1.524	1.526	1.526	1.536	1.528 (6)
C21–C23	1.516	1.516	1.517	1.525	1.519 (6)
C14–O4	1.422	1.423	1.423	1.410	1.429 (6)
C15–O5	1.422	1.422	1.422	1.421	1.425 (5)
C16–O6	1.420	1.422	1.422	1.421	1.410 (6)
C17–O7	1.420	1.420	1.410	1.422	1.435 (5)
C18–O8	1.418	1.418	1.417	1.425	1.412 (5)
C19–O9	1.418	1.419	1.420	1.418	1.411 (6)
C22–O10	1.416	1.418	1.418	1.417	1.425 (5)
C23–O11	1.422	1.421	1.420	1.423	1.429 (6)
RMSD	**0.011**	**0.011**	**0.013**	**0.014**	
Dihedral angles (°)					
C12–O1–C13	114.4	114.2	114.3	115.5	115.7 (3)
C12–O2–C20	116.2	116.5	116.3	115.0	114.1 (3)
C13–O3–C21–	115.8	115.9	114.7	114.9	114.3 (3)
C12–C14–C16	110.6	110.9	111.0	110.0	109.5 (4)
C14–C16–C18	110.9	110.3	110.4	109.3	108.6 (4)
C16–C18–C20	109.2	109.6	109.5	109.5	113.1 (4)
C18–C20–O2	109.5	112.3	112.0	108.8	111.6 (4)
O2–C12–O1	112.5	112.7	112.5	111.6	111.9 (1)
O1–C13–O3	112.5	112.6	112.3	112.4	111.3 (4)
C20–C22–O10	111.2	111.1	111.0	114.2	112.9 (4)
O1–C12–C14	106.1	106.3	106.1	107.5	106.4 (1)
O1–C13–C15	106.3	106.2	106.6	106.3	105.9 (4)
C13–C15–C17	110.4	110.4	111.3	110.2	110.3 (4)
C15–C17–C19	111.0	111.0	110.3	111.3	112.2 (4)
C17–C19– C21	108.8	108.9	107.4	109.1	110.7 (4)
C19–C21–O3	109.2	109.3	108.0	107.9	112.6 (4)
C21–C23–O11	107.6	107.6	107.5	113.9	112.1 (4)
RMSD	**2.1**	**2.0**	**2.3**	**1.8**	
Dihedral angles (°)					
C13–O1–C12–O2	68.0	70.9	65.4	79.2	75.0
C12–O1–C13–O3	62.8	65.3	64.5	68.8	61.7
O2–C12–C14–C16	50.8	53.5	52.7	51.4	62.7
C12–C14–C16–C18	−52.4	−54.5	−53.6	−53.5	−56.8
C16–C18–C20–O2	−56.4	−51.9	−52.8	−59.5	−47.9
C18–C20–O2–C12	58.7	54.0	55.1	59.0	53.9
C18–C20–C22–O10	177.9	−177.7	−178.6	33.2	47.4
O3–C13–C15–C17	50.5	50.6	48.9	52.2	55.5
C13–C15–C17–C19	−51.8	−51.9	−51.0	−52.5	−51.6
C17–C19–C21–O3	−57.6	−57.1	−61.9	−58.2	−50.2
C19–C21–O3–C13	60.1	59.6	63.7	62.4	60.0

(*continued on next page*)

Table 2 (*continued*)

B3LYP/6-31G*[a]					
Parameter	Anhydrous			Dihydrated	
	α-α-trehalose	α-β-trehalose	β-β-trehalose	α-α-trehalose	Exp[b] α-α-trehalose
C19–C21–C23–O11	−169.8	−170.1	−170.7	−170.6	−167.7
O1–C13–C15–O5	52.0	51.8	51.1	53.8	
O2–C20–C22–O10	57.8	59.0	58.4	–87.5	
O3–C21–C23–O11	69.5	69.1	69.9	69.9	
O1–C12–C14–O4	52.4	55.1	54.6	48.8	
C16–C14–C12–O1	−72.0	−69.5	−70.2	−71.8	
O1–C12–O2–C20	63.4	65.4	65.0	65.4	
RMSD	**38.1**	**65.1**	**65.5**	**7.4**	

Bold letter: RMSD values.
[a] This work.
[b] Ref (Brown et al., 1972).

(Tomasi and Persico, 1994; Miertus et al., 1998; Marenich et al., 2009) are summarized in Table 3. The results for all the trehalose species show expansions of volume in aqueous solution where the value increases according to the following order: αβ-trehalose (1.4 Å^3) < αα-trehalose (2.1 Å^3) < ββ-trehalose (2.8 Å^3). This variation observed could suggest that the position of the OH group also has influence on the volume variation, thus when the position is ββ- the variation is higher. This way, the reduction in their dipole moment value could justify that observation. On the other hand, the volume expansions theoretically observed for trehalose, maltose and sucrose could probably explain that different water molecules are around disaccharide–water mixtures which generate a particular higher "rigidity" in trehalose due to their lower volume variation, as was experimentally observed by Varga et al. (2008). A similar relation is observed in the calculated solvation energy values, as indicated in Table 3. Thus, the species with higher volume variation, it is the ββ-trehalose form, present the higher solvation energy value, probably because only for this species in solution the dipole moment values significantly decrease their value from 2.72 D in gas phase to 0.81 D in solution while for the remain species the values increase in this medium. When these values are compared with the values corresponding to the two maltose anhydrous species we observed a contrary relation because the species with higher volume variation present the lower solvation energy value. On the other hand, when the solvation energies for the trehalose species are compared with the other sugars, we observed that the β anhydrous and monohydrated species have higher values than the corresponding α ones where, in particular, the values of the hydrated sugar species decreasing according to the following order: Sucrose dihydrated > β-maltose > Anhydrous sucrose > Anhydrous β-Lactose > Sucrose pentahydrated > Anhydrous α-Lactose > α-α-trehalose dihydrated > α-Lactose Monohydrated > Anhydrous maltose while the three anhydrous species of trehalose have the lowest solvation energy values, as observed in Table 3. These low solvation energies values observed for trehalose in relation to sucrose and maltose probably can explain in part why a trehalose/water mixture shows a larger structural resistance to temperature changes and a higher "rigidity" in comparison with maltose/H_2O and sucrose/H_2O mixtures, as mentioned by Varga et al. (2008). This property of trehalose could also be related to the most intense disaccharide–water interaction observed for trehalose by Magazù et al. (2007).

4.3. Charges, molecular electrostatic potentials (MEP) and bond orders (BO) studies

For the four trehalose forms, two charge's types, the atomic MK and NPA charges (Besler et al., 1990; Glendening et al., 1996), were considered using the B3LYP/6-31G*Method, as was mentioned in section computational details. These charges for those species in gas phase are summarized in Table S1 while the values in solution are given in Table S2. The exhaustive inspection of the values show that the NPA charges have in general higher values than the MK charges in both media and besides, these charges on the C22 and C23 atoms in the four species have negative signs, as observed in Tables S1 and S2. Note that the MK charge on the C19 atom belonging to the R1 ring of the dihydrated species present negative sign in gas phase and positive in solution while on the other ones are observed positive sings. On the other hand, these charges in solution are observed with negative signs on the C12 and C13 atoms in the dihydrated species while in gas phase on both atoms are observed positive signs. Note that for the dihydrated species in gas phase we observed positive signs in both charges on all the H atoms corresponding to the water molecules. On the contrary, in solution the NPA charges on the H atoms of the dihydrated species are observed with negative signs while the MK exhibits in this media positive signs. These variations in the charges observed for the species in solution could clearly explain the hydration process with water molecules of the solvent. Besides, these changes in the charges possibly will explain the most intense disaccharide–water interaction observed for trehalose in solution by Magazù et al. (2007) that moreover will justify their higher bioprotective effectiveness.

The MEPs were analyzed on all the atoms of the four species in both media and the corresponding values are presented in Table S3. Analyzing the results, we observed that in both media the most negative values are located on the O10 atoms of all the species while the less negative values for the anhydrous species are observed on the O1 atoms and for the dihydrated species on the O3 atom. Thus, these results for the

Table 3 Molecular volume and calculated solvation energies (ΔG) for the studied anhydrous and dihydrated species derived from trehalose in different media using the B3LYP/6-31G* method.

Molar Volume (Å^3)			
Trehalose Anhydrous[a]			
Species	GAS	PCM/SMD	$^{\#}\Delta V = V_{AS}–V_G$ (Å^3)
α-α-trehalose	327.1	329.3	2.1
α-β-trehalose	322.4	323.8	1.4
β-β-trehalose	320.9	323.7	2.8
Trehalose dihydrated[a]			
α-α-trehalose	357.8	359.7	1.9
Solvation energies (kJ/mol)			
Trehalose Anhydrous[a]			
Species	$\Delta G_u{}^{\#}$	ΔG_{ne}	ΔG_c
α-α-trehalose	−142.95	25.87	−168.82
α-β-trehalose	−142.28	25.66	−167.88
β-β-trehalose	−155.81	25.29	−181.10
Trehalose dihydrated[a]			
α-α-trehalose	−169.18	29.97	−199.15
Maltose Anhydrous[b]			
α-maltose	322.1	325.6	3.5
β-maltose	322.7	325.1	2.4
Maltose Monohydrated[b]			
α-maltose	343.6	348.7	5.1
β-maltose	342.9	344.7	1.8
Solvation energies (kJ/mol)			
Species	$\Delta G_u{}^{\#}$	ΔG_{ne}	ΔG_c
Maltose Anhydrous[b]			
α-maltose	−151.87	25.29	−177.16
β-maltose	−158.43	23.99	−182.42
Maltose Monohydrated[b]			
α-maltose	−157.64	31.43	−189.07
β-maltose	−185.97	24.79	−210.76
Lactose Anhydrous[c]			
α-Lactose	−174.95	26.33	−201.28
β-Lactose	−179.67	26.17	−205.84
Lactose Monohydrated[c]			
α-Lactose	−165.25	30.18	−195.43
Sucrose[d]			
Anhydrous	−182.00	28.38	−210.38
Sucrose.$(H_2O)_2$	−198.56	29.30	−227.86
Sucrose.$(H_2O)_5$	−160.00	41.97	−201.97

$\Delta G_c = \Delta G$uncorrected$^{\#} - \Delta G$Totalnon electrostatic.
$^{\#}$ AS, aqueous solution; G, gas phase.
[a] This work.
[b] From Ref. Iramain et al. (2016).
[c] From Ref. Márquez et al. (2015a,b).
[d] From Ref Brizuela et al. (2014).

anhydrous species could indicate that the inter-ring C13-O1–C12 angle is independent of the medium employed. Besides, this result probably is also related to that observed experimentally by Taga et al. (1972) for the dihydrated species because neither the ring oxygens nor the glycosidic linkage oxygen accept hydrogen bonds. Later, as it is expected, the lowest negative MEP values for all the trehalose species are observed on the H atoms where the anhydrous species show the highest values on the H34 atoms while the lower values are observed on the H38 and H39 atoms of these species probably because the distances between these atoms are close to the corresponding O1 atoms (2.248–2.241 Å) and, for these reasons, they are the more labile atoms. Analyzing, the values for the dihydrated species, the higher values are also observed on the H34 atoms while the lowest values on the H atoms of the water molecules. The different reaction sites can be obviously observed by the different colorations when the MEP mapped surfaces for the α-α-anhydrous and dihydrated species are compared in Fig. S2. Thus, the blue colors show the electrophilic sites observed on the H atoms while the nucleophilic sites are clearly observed in red color on all the O atoms. Here, it is interesting to note that in the dihydrated species a strong blue color are observed on the H atoms of the water molecules in agreement to the low MEP values, as observed in Table S3.

In relation to the bond order values, Table S4 show these values expressed as Wiberg indexes, for the four trehalose species. The results clearly show that for the four species the higher BO values are observed in the O atoms that belong to the R1 and R2 rings and to the inter-ring O atoms, these are the O1, O2 and O3 atoms, which have values between 2,030 and 1,978 while their values clearly decrease in solution. Here, newly we evidenced that experimental results found by Taga et al. (1972) for the dihydrated species. On the contrary, in general remaining O atoms of all the species belonging to different OH groups in the two rings are observed slight increase in the BO values in solution. These higher values in solution probably indicate that these H atoms linked to those O atoms are less labile. On the contrary, regarding the BO values for the C atoms, the C16 and C17 atoms in αα-trehalose and the C17 atoms in αβ and ββ-trehalose and the C14 and C19 atoms in the dihydrated species present the higher values in gas phase but, some of these values change few in solution. Probably, due to the different positions of the OH groups linked to the C atoms some values for these atoms are different in the four species. Other very important result is observed in the H atoms of the four species because when those atoms are linked to the C atoms have higher values than the other ones, as expected due to that the H atoms bonded to the OH groups are most labile and, as a consequence they have the lowest values. An expected result is observed in the dihydrated species, because the O and H atoms belonging to the water molecules present the lowest BO values but, they increase notably in solution due to the hydration of these atoms with water molecules. These results can explain that the water mobility within the first hydration shell is ca. 25% smaller than that of pure water, as observed by Bonanno et al. (1998) from molecular dynamics simulation studies for the water interaction with αα-trehalose.

4.4. Stability study

The stabilities of all the trehalose's species in gas and aqueous solution phases were studied using NBO (Glendening et al., 1996) and AIM (Biegler-Köning et al., 2001) calculations. Thus, the donor–acceptor interaction energies obtained from the second order perturbation calculations in those media are presented in Table S5. Here, the main donor–acceptor interaction energies for the anhydrous species in both media are observed from the lone pairs of the O atoms to the anti-

bonding O–C orbitals ($LP(2)O1 \rightarrow \sigma^*O–C$) while for the dihydrated species besides these are also observed those from the lone pairs of the O atoms to the antibonding O–H orbitals ($LP(2)O1 \rightarrow \sigma^*O–H$), as can be seen in Table S5. Thus, the contributions to the total energy show clearly that the dihydrated species are the most stable in both media than the anhydrous species. The presence of a additional H bonds interaction in solution in the dihydrated species will explain perhaps the role of trehalose in the stabilization of proteins because, as recently was mentioned by Olsson et al. (2016), the protein adsorbs water and thereby reduces the water content in the trehalose–water system.

The stabilities of all the trehalose's species were also studied by means of the topological properties with the AIM2000 program (Biegler-Köning et al., 2001). Accordingly, the calculated charge electron density, (ρ) and the *Laplacian* values, $\nabla^2\rho(r)$ in the bond (BCPs) and ring critical points (RCPs) for the R1 and R2 rings of the three anhydrous and dihydrated species in both media are given in Tables S6 and S7, respectively. Analyzing first the three anhydrous species we observed from Table S6 notable differences between the values in gas phase and those in solution. For instance, the αβ- and ββ- species in gas phase present the two expected RCPs due to the R1 and R2 rings and the H bonds O6–H42 interactions while this latter interaction it is not observed in the αα- species. On the contrary, in solution the αα- and αβ- species have the two RCPs and a new H–H interaction while in the ββ- species there is not observed the latter interaction. This observation can be justified by the large distance between the O6 and H42 atoms of 3.519 Å. On the other hand, the distance between the H33 and H38 atoms of 2.615 Å justifies that in the αα species in gas phase there is not observed interaction between both atoms. For the dihydrated trehalose species a very different situation is found when their topological properties are analyzed in gas and in aqueous solution phases. Thus, Table S7 shows their calculated properties using the B3LYP/6-31G* Method in both media. First, in both media are observed the two RCPs but in gas phase are observed six O–H interactions while in solution are observed only five because the O8–H44 interaction in solution present a distance of 3.139 Å. These results clearly show the high stability of the dihydrated species in both media and, besides, suggest the presence of this species in the solid state, in complete agreement with the NBO results. Here, another very important result is the formation of the H bond O3–H49 interactions in both media observed only for the dihydrated species because this O3 atom belong to the glucopyranose R1 ring. This result is different from that observed experimentally by Taga et al. (1972) for the dihydrated species where neither the ring oxygens nor the glycosidic linkage oxygen accept hydrogen bonds. The AIM study explains the ability of trehalose to form H bonds and, this way, to stabilize the membranes, as reported by Crowe and Crowe (1984).

The high stability of the dihydrated trehalose species predicted using NBO and AIM studies, as compared with the anhydrous species due to the H bonds formation could support: (i) the small perturbation of water hydration shell and short hydrogen bonds between trehalose oxygens and water hydrogens (Pagnotta et al., 2008), (ii) the water dynamics in the presence of bioprotectant systems which is affected by all the disaccharides and particularly by trehalose (Varga et al., 2008; Magazù et al., 2007), (iv) that trehalose is shown to affect the swelling properties of the polymer with temperature, stabilizing its conformation (Magazù et al., 1998), (v) the presence of the disaccharides inhibits the protein dynamical transition (Magazù et al., 2011) and, (vi) only the H bonds intra-molecular, as mentioned by Ballone et al. (2000), because the DFT results for the isolated molecule is a simplified scheme and provides a fairly good description of ground-state geometries. On the contrary, the cohesion of the crystal is mainly due to the formation of several intermolecular hydrogen bonds which involve every hydroxyl group in the system.

4.5. Frontier orbitals and descriptors study

Trehalose is a sugar that acts on the stability of membranes in anhydrobiotic organisms and this effect is only observed in this carbohydrate by Crowe and Crowe (1984), for this reason, it is very important to predict their reactivities and behaviors in gas and in aqueous solution in order to understand their mechanism of bio-protecting. Thus, their reactivities in those media were predicted using the frontier orbitals (Parr and Pearson, 1983; Brédas, 2014; Márquez and Brandán, 2014; Cataldo et al., 2014; Romani and Brandán, 2015a; Romani et al., 2015b), whose values are presented in Table S8, while the chemical potential (μ), electronegativity (χ), global hardness (η), global softness (S), global electrophilicity index (ω) and mucleophilic index (E) descriptors were employed (Márquez and Brandán, 2014; Cataldo et al., 2014; Romani and Brandán, 2015a; Romani et al., 2015b; Márquez et al., 2015a,b) to predict their behaviors in the two media and, they are summarized in Table S9. These properties calculated for the trehalose species were then compared with those reported for maltose and lactose (Iramain et al., 2016). Here, the high gap values observed for the anhydrous and dihydrated species of trehalose could probably explain that it is a no reducing disaccharide of glucose while the similar lower gap values for maltose and lactose probably justify that these carbohydrates are reducing sugars. Note that the reactivity in all the sugars increases in aqueous solution. In particular, if trehalose is less reactive in water in a protein–trehalose–water system the protein adsorbs water decreasing their content from the trehalose–water system, as reported by Olsson et al. (2016). Moreover, the major intensity in the trehalose–water interaction and its higher bioprotective effectiveness, as mentioned by Magazù et al., 2007 could also be justified by the high gap value and low reactivity. On the other hand, the high gap values observed for the anhydrous and dihydrated species of trehalose suggest a reduced reactivity that could support that this species acts as a nonreducing disaccharide of glucose while the similar lower gap values for maltose and lactose probably justify that these carbohydrates are reducing sugars. Here, it is necessary to remember that in a reducing disaccharide of glucose (maltose) one of the two monosacharides has one free hemiacetal unit that generates a reducing aldehyde group while the other one is occupied with the glycosidic bond which cannot act as reducing agent. On the contrary, trehalose is a nonreducing disaccharide of glucose because there is not a free hemiacetal unit but there is an acetal linkage between their anomeric centers, giving a structure without one free hemiacetal unit to act as reducing agent.

In relation to the descriptors, it is necessary to clarify that as their equations are widely known these were not included in the main manuscript but in Table S9. Regarding exhaustively the

descriptors, we observed first that all the values observed in gas phase decrease in solution and, then, that the less reactive species (> gap) are the trehalose's species which have > global hardness (η) and < global softness while the anhydrous species also present > nucleophilic and electrophilic indexes. Analyzing the nucleophilic and electrophilic indexes for the hydrated disaccharides in solution, we observed that the presence of two water molecules in trehalose, in relation to one in maltose and lactose, increase the nucleophilicity thus, the observed tendency is: trehalose > maltose > lactose while the trend change with the electrophilicity to: maltose > trehalose > lactose. These results are in agreement with those MEP values predicted for the nucleophilic sites on all the O atoms including all OH groups and, with the results suggested by Ballone et al. (2000), because the cohesion of the crystal is mainly due to the formation of several intermolecular hydrogen bonds which involve every hydroxyl group in the system. The nucleophilicity index observed especially in the hydrated species could probably be related with that important property to stabilize membranes due to their ability to form H bonds and, hence, to replace water around the head group of a phospholipid, according to the results observed by Crowe and Crowe (1984). In addition, that nucleophilicity index will explain why trehalose inhibits the protein dynamical transition during the addition of disaccharides to hydrated lysozyme and why the of hydrogen bond connectivity has influence on transport properties for the trehalose–water system, as revealed by Magazù et al. (2011) and 1998, respectively.

4.6. Vibrational analysis

All the trehalose species were optimized using B3LYP/6-31G* calculations with C_1 symmetry where the three anhydrous species have 129 normal vibration modes while the dihydrated species present 147 normal vibration modes and, where all these modes show activity in the infrared and Raman spectra. The experimental infrared and Raman spectra of dihydrated trehalose in the solid phase can be seen in Fig. 4 while in Fig. 5 is presented a comparison of the IR spectrum of the αα-dihydrated species with the corresponding predicted for this species and their dimer in gas phase at the B3LYP/6-31G* level of theory. On the other hand, Fig. S3 shows the comparisons among the experimental IR of dihydrated trehalose in the solid phase with the corresponding predicted for the three anhydrous species in gas phase using that level of theory. The comparisons among the experimental IR of dihydrated trehalose in the solid phase in the 4000–2500 cm^{-1} region with the predicted for this species and their corresponding dimer in gas phase at the same level of theory are given in Fig. S4 while in Fig. S5 are presented these same comparisons but in the 2000–0 cm^{-1} region. These two comparisons clearly evidence the presence of more than one molecule in the solid state due to the increase in the numbers and intensities of the bands in both spectra for this species in relation to the observed in the dihydrated species. A similar situation is observed when the Raman spectra are compared in those two regions, as can be seen in Fig. S6 and S7. In the 4000–2500 cm^{-1} region the presence of a dimer is also observed in the form of the bands with higher intensities (Fig. S6, green spectrum) while the quantities and forms of the bands in the 2000–0 cm^{-1} region could support the presence of the dimer, as those two most intense bands are observed in the Raman spectra at approximately 1500 cm^{-1}. In Table 4 is summarized the observed and calculated

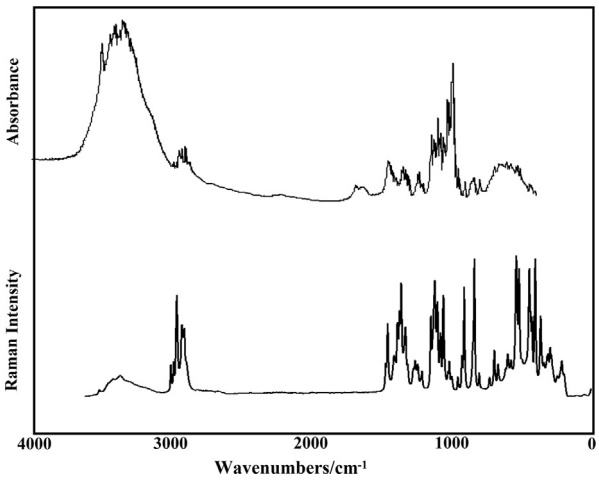

Figure 4 Experimental FTIR spectrum of αα-dihydrated in the solid phase in the 4000–400 cm^{-1} region compared with their corresponding FT-Raman spectrum in the 4000–10 cm^{-1} region.

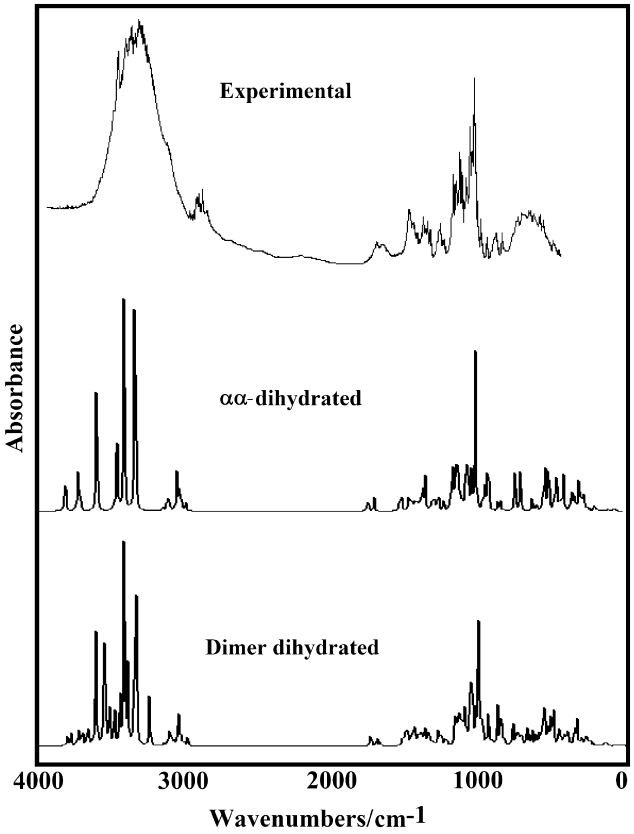

Figure 5 Experimental FTIR spectra of αα-dihydrated in the solid phase compared with the corresponding predicted for this species and their dimer in gas phase at the B3LYP/6-31G* level of theory.

wavenumbers and assignments for the three anhydrous and dihydrated species in gas phase using SQM/B3LYP/6-31G* calculations while for the assignments of the dimer the *GaussView* program (Nielsen and Holder, 2008) was used. We observe from Table 4 that the assignments are clearly different for the αα-, αβ- and ββ-trehalose species indicating, this way, the influence of the position of the OH groups on the bands observed in both spectra. Here, the SQM force fields were calculated with the Molvib program (Sundius, 2002) using scale factors valid for B3LYP/6-31G* calculations (Rauhut and Pulay, 1995a,b). These results can be obtained at the request of the authors. On the other hand, the vibrational assignments for the anhydrous and dihydrated species were performed taking into account those assignments reported for other sugars (Brizuela et al., 2012a, 2014; Márquez et al., 2015a,b; Iramain et al., 2016), those reported by Takahashi et al. (2006) for the low-frequency vibrations of the dihydrated species and, in accordance with ours DFT calculations obtained here. It is necessary to clarify that Ballone et al. (2000) have studied structural properties and harmonic vibrational modes of trehalose in the gas phase and in the monohydrate crystal in order to analyze the local conformation and the relative strength of intra- and intermolecular hydrogen bonds, and the effects of the crystal environment on the molecular geometry and vibrational frequencies. Their results provide a fairly good description of ground-state geometries, while vibrational properties are only in qualitative agreement with those computed by the density functional method.

Later, the assignments for some groups are presented below.

4.6.1. Band assignments

4.6.1.1. O–H modes. For the four trehalose species, the B3LYP/6-31G* calculations predicted these stretching modes as nearly pure modes, hence, due to the form of the bands and to their intensities these vibration modes for the anhydrous species can be easily assigned to the broad IR and Raman bands located in the 3500–3160 cm^{-1} region, as observed in Table 4. Besides, in the dihydrated species in that region are also expected the four antisymmetric and symmetric OH stretching modes corresponding to the two water molecules. Thus, the IR bands at 3500, 3444 and 3335 cm^{-1} are associated with those vibration modes for the hydrated species while, for the dimer, the band at 3374 cm^{-1} and the shoulder at 3269 cm^{-1} in the same spectrum are also related to those stretching modes. Here, the different positions predicted for these vibration modes in the hydrated species could probably reveal forming the H bonds, as supported by the NBO and AIM calculations (Tables, S5, S6 and S7) and, as also was observed in the maltose species (Iramain et al., 2016). The intra-molecular O–H stretching modes are particularly sensitive to environmental modifications, as reported by Branca et al., 1999 from viscosity and Raman scattering studies and, as will be seen later, the force constants related to this stretching mode is lower in the dihydrated trehalose species, in reference to maltose and lactose.

Here, the OH deformation modes of the water molecules for the hydrated and the dimer species are clearly assigned to the IR bands at 1687 and 1639 cm^{-1}. The OH deformation modes for all the species are predicted between 1419 and 1194 while in the anhydrous species of maltose those modes appear in the 1421–1171 cm^{-1} region (Iramain et al., 2016), therefore, these modes can be associated with observed bands in that region. In general, the calculations predict the out-of-plane deformation modes for the dihydrated species strongly mixed with other vibration modes, such as deformations, stretching and rocking modes of the OH, CH_2, C–O and C–H groups, as shown in Table 4. Note that the out-of-plane deformation modes in the anhydrous forms appear at lower wavenumbers (476 up to 189 cm^{-1}) while in the dihydrated species these modes are also predicted in the higher wavenumbers region (from 1389 up to 163 cm^{-1}). In the anhydrous forms of maltose these modes are assigned between 537 and 182 cm^{-1} while for the monohydrated species the bands between 884 and 107 cm^{-1} are associated to those modes. The comparisons between the experimental IR and Raman spectra with the corresponding theoretical in the different regions (Figs. S4–S7) support the presence of more than one molecule in the primitive cell due to the increase in the numbers and intensities of the bands in both spectra for this species in relation to the observed in the dihydrated species.

4.6.1.2. CH modes. In sucrose, lactose and maltose these stretching modes were assigned to the bands observed in the 3094/2830, 3086/2881 and 2982/2845 cm^{-1} regions (Brizuela et al., 2012a, 2014; Márquez et al., 2015a,b; Iramain et al., 2016), respectively while in the trehalose species these modes are predicted between 2997 and 2821 cm^{-1}. The Raman band of medium intensity at 2997 cm^{-1} is associated to the symmetric modes corresponding to the dihydrated and dimeric species. In the lactose species, the rocking modes are assigned between 1469 and 1212 cm^{-1} while in maltose are assigned to the bands between 1457 and 1063 cm^{-1}. In the trehalose species, these modes are predicted between 1434 and 1180 cm^{-1}.

4.6.1.3. CH_2 modes. In maltose, the antisymmetric and symmetric stretching modes are assigned respectively to the pairs of bands at 3032/2970 and 2963/2862 cm^{-1} (Iramain et al., 2016) while in the four species of trehalose these modes are predicted at 3153/2881 cm^{-1}. Obviously, the symmetric modes are observed with higher intensities in the Raman spectrum and, for this reason, they are assigned to the Raman band at 2997 cm^{-1}. In lactose, the deformation or scissoring modes are assigned at 1457/1367 cm^{-1} (Márquez et al., 2015a,b), in the maltose species these modes are assigned at 1499/1455 cm^{-1} (Iramain et al., 2016) while in trehalose species they are assigned at 1469/1451 cm^{-1}. The wagging, rocking and twisting modes are predicted by calculations between 1451/1405 and in some cases coupled at 1268 cm^{-1}, 1265/1211 and 1069/777 cm^{-1}, respectively as indicated in Table 4. This way, they are assigned accordingly.

4.6.1.4. Skeletal modes. The C–O stretching modes belonging to the two glucopyranose R1 and R2 rings and to the glycosidic C12–O1–C13 bonds are predicted by calculations in different regions and mixed with other vibration modes, as can be seen in Table 4. Thus, these modes for the anhydrous and dihydrated species can be observed from 1132 to 744 cm^{-1}. Note that the C12–O2 and C13–O3 stretching modes are predicted at higher wavenumbers in the four species than the C12–O1 and C13–O1 stretching modes, as expected because these stretching modes are related to the glycosidic C12–O1–C13 bonds which present different values for the anhydrous and dihydrated species, as shown Table 2. In the maltose species,

Table 4 Observed and calculated wavenumbers (cm^{-1}) and assignments for the five trehalose species studied.

Experimental[a]		Ref[c]	Anhydrous[a]						Dihydrated[a]			
IR	Raman	IR	αα-Trehalose		αβ-Trehalose		ββ-Trehalose		αα-Trehalose		Dimer	
Solid	Solid	Solid	SQM[b]	Assig	SQM[b]	Assig	SQM[b]	Assig	SQM[b]	Assig	Calc.	Assig
3500 w	3504 w		3606	ν(O11–H45)	3606	ν(O11–H45)	3609	ν(O11–H45)	3651	ν_aH_2O(W1)	3798	ν_aH_2O
			3580	ν(O10–H44)	3582	ν(O10–H44)	3585	ν(O10–H44)	3647	ν_aH_2O(W2)	3604	ν_sH_2O
			3574	ν(O8–H42)	3570	ν(O9–H43)	3565	ν(O4–H38)	3569	ν(O7–H41)	3608	ν(O–H)
			3570	ν(O9–H43)	3565	ν(O7–H41)	3562	ν(O5–H39)	3569	ν(O8–H42)	3604	ν_sH_2O
			3565	ν(O7–H41)	3561	ν(O4–H38)	3561	ν(O9–H43)	3568	ν(O9–H43)	3547	ν(O–H)
			3565	ν(O6–H40)	3558	ν(O5–H39)	3554	ν(O7–H41)	3565	ν(O10–H44)	3536	ν(O–H)
			3562	ν(O4–H38)	3548	ν(O6–H40)	3550	ν(O6–H40)	3557	ν(O6–H40)	3511	ν_aH_2O
3474 sh			3559	ν(O5–H39)	3540	ν(O8–H42)	3542	ν(O8–H42)	3552	ν(O5–H39)	3479	ν(O–H)
3444 w									3445	ν_sH_2O(W1)	3442	ν_aH_2O
3374 s											3388	ν_aH_2O
3357 s	3350 w,br										3347	ν(O–H)
3335 s									3312	ν_sH_2O(W2)		
3321 w	3323 sh								3265	ν(O11–H45)		
3269 sh	3280 sh								3193	ν(O4–H38)	3242	ν(O–H)
3153 sh	3137 sh										3049	ν_sCH_2(C23)
2995 w	2997 m	**2993**	3011	ν_sCH_2(C22)	2996	ν(C12–H24)	2997	ν(C12–H24)			3047	ν_sCH_2(C23)
2995 w	2997 m	**2993**			2988	ν_sCH_2(C22)	2990	ν_sCH_2(C22)	3008	ν_sCH_2(C23)	3032	ν_aCH_2(C23)
2995 w	2997 m	**2993**	2995	ν(C12–H24)	2988	ν(C14–H26)	2988	ν(C14–H26)	2989	ν_sCH_2(C22)	3030	ν_aCH_2(C23)
	2988 sh		2984	ν(C13–H25)	2983	ν(C13–H25)	2985	ν(C13–H25)	2980	ν(C12–H24)	2984	ν(C–H)
2973 w	2973 m	**2973**	2969	ν(C14–H26)			2970	ν(C15–H27)	2972	ν(C15–H27)	2982	ν(C–H)
		2957	2967	ν(C15–H27)	2968	ν(C15–H27)	2961	ν(C19–H31)	2962	ν(C21–H33)		
2951 w	2953 m	**2950**	2942	ν_sCH_2(C23)	2940	ν(C21–H33)	2942	ν_aCH_2(C23)	2958	ν(C13–H25)		
	2941 sh	**2943**	2934	ν(C20–H32)	2930	ν_aCH_2(C22)	2932	ν_aCH_2(C22)				
2934 w		**2934**	2930	ν(C21–H33)	2929	ν_sCH_2(C23)	2928	ν(C21–H33)	2920	ν(C18–H30)		
2908 w	2916 m	**2908**			2914	ν(C20–H32)	2914	ν(C20–H32)	2911	ν_aCH_2(C22)		
	2900 m	**2897**							2903	ν_aCH_2(C23)		
2881 w	2886 sh	**2880**	2885	ν_aCH_2(C23)	2883	ν_aCH_2(C23)	2881	ν_sCH_2(C23)	2898	ν(C14–H26)		
2881 w	2886 sh		2877	ν_aCH_2(C22)					2896	ν(C20–H32)		
2861 sh	2859 sh		2873	ν(C19–H31)	2873	ν(C16–H28)	2873	ν(C16–H28)	2889	ν(C17–H29)		
2861 sh	2859 sh		2869	ν(C18–H30)	2872	ν(C19–H31)			2880	ν(C16–H28)		
	2852 sh		2859	ν(C17–H29)	2859	ν(C17–H29)	2859	ν(C18–H30)	2859	ν(C19–H31)		
2837 sh			2857	ν(C16–H28)	2858	ν(C18–H30)	2821	ν(C17–H29)				
1687 w	1684 vw	**1689**							1660	δH_2O(W2)	1697	δH_2O
1639 w,br	1613 vw								1623	δH_2O(W1)	1675	δH_2O
	1469 w		1481	δCH_2 (C23)	1481	δCH_2 (C23)	1473	δCH_2 (C23)	1475	τO4–H38 τO47–H38	1516	δCH_2
		1460	1462	δCH_2(C22)	1461	δCH_2(C22)	1462	δCH_2(C22)	1465	τO4–H38 τO47–H38	1494	δ(O–H)
1457 m									1452	δCH_2(C22)	1455	ρC–H
1451 m	1452 s		1453	$wagCH_2$(C23) ν(C21–C23)	1454	ν(C21–C23)	1457	$wagCH_2$(C23)	1451	δCH_2 (C23) δ(O11–H45)	1453	$wagCH_2$

(*continued on next page*)

Table 4 (*continued*)

Experimental[a]		Ref[c]	Anhydrous[a]						Dihydrated[a]			
IR	Raman	IR	αα-Trehalose		αβ-Trehalose		ββ-Trehalose		αα-Trehalose		Dimer	
Solid	Solid	Solid	SQM[b]	Assig	SQM[b]	Assig	SQM[b]	Assig	SQM[b]	Assig	Calc.	Assig
1429 w			1431	wagCH_2(C22)	1428	wagCH_2(C22) ν(C20–C22)	1433	ρC15–H27	1434	ρC18–H30 ρC16–H28 δ(O6–H40)	1434	ρC–H
1429 w			1425	ρC14–H26 ρC15–H27	1423	ρC15–H27 wagCH_2(C22)	1429	wagCH_2(C22)	1427	ρ'C21–H33	1428	ρC–H
1429 w			1423	δ(O9–H43) ρC19–H31	1422	δ(O9–H43) ρ'C19–H31	1422	ρC14–H26	1426	ρ'C18–H30	1426	ρC–H
1429 w			1420	ρC17–H29	1419	ρC17–H29			1424	ρC17–H29 ρC15–H27	1422	wagCH_2
	1417 sh		1417	wagCH_2(C22) ρC16–H28	1417	δ(O8–H42)	1419	δ(O8–H42)	1418	δ(O5–H39)	1419	wagCH_2
	1417 sh		1415	ρC14–H26 ρC16–H28	1414	ρC15–H27 ρC17–H29	1415	ρC19–H31			1417	ρC–H
1410 sh	1410 m		1411	ρC15–H27			1408	ρC19–H31 ρ'C16–H28	1410	wagCH_2(C23)	1413	ρC–H
	1405 sh				1406	δ(O4–H38) ρC14–H26	1404	δ(O7–H41)	1405	wagCH_2(C22) δ(O10–H44)	1409	ρC–H
1400 w							1397	ρC17–H29	1398	ρ'C12–H24 ρC13–H25	1398	ρC–H
	1392 sh		1394	ρ'C12–H24 ρC13–H25	1392	ρ'C12–H24	1392	ρ'C12–H24 ρC13–H25	1389	τCO4–H38 τO47–H38	1388	ρC–H
1385 w	1384 s		1386	ρ'C12–H24 ρC16–H28	1384	ρ'C12–H24			1384	τCO4–H38 τO47–H38	1387	ρC–H
1385 w	1384 s		1383	ρ'C12–H24	1378	ρC20–H32 ρC13–H25	1383	ρC20–H32	1381	τCO4–H38 τO47–H38	1380	ρC–H
1373 sh	1374 sh		1375	δ(O10–H44)	1376	ρC16–H28 δ(O10–H44)	1379	δ(O10–H44)	1374	τCO4–H38 τO47–H38	1375	ρC–H
1371 w	1370 s		1371	ρ'C13–H25	1372	δ(O10–H44) ρC18–H30	1376	ρC16–H28			1371	ρC–H
	1363 sh	**1365**			1367	ρ'C13–H25	1368	ρ'C13–H25	1362	ρ'C13–H25 ρC21–H33	1366	ρC–H
1356 m	1357 vs		1360	ρC12–H24			1361	ρ'C21–H33	1357	ρC12–H24	1359	ρC–H
1349 sh	1350 sh				1355	ρC13–H25	1356	ρC21–H33 ρ'C21–H33			1355	ρC–H
	1348 sh		1354	ρC21–H33	1353	ρC21–H33	1347	ρC18–H30	1348	ρC21–H33 ρC13–H25	1349	ρC–H
1342 vw			1343	ρC18–H30	1345	ρC20–H32 ρC18–H30	1344	ρC21–H33	1345	ρC14–H26 ρ'C14–H26	1348	ρC–H
	1336 sh	**1333**	1335	ρC19–H31	1337	ρC19–H31			1338	ρC19–H31	1333	ρC–H
1333 w	1330 sh		1331	ρC13–H25	1332	ρC12–H24			1338	ρC20–H32	1324	ρC–H
	1328 s		1323	ρC20–H32			1337	ρC12–H24	1330	τCO4–H38 τO47–H38	1319	ρC–H

	1328 s		1318	ρ'C21–H33 δ(O7–H41)	1316	ρ'C21–H33	1305	ρ'C14–H26	1317	ρ'C21–H33	1317	δ(O–H)
1311 w	1314 w	**1312**	1308	ρ'C20–H32 δ(O8–H42)	1303	ρ'C14–H26	1297	ρ'C15–H27 ρ'C19–H31	1314	ρ'C20–H32 δ(O8–H42)	1307	δ(O–H)
1294 sh			1297	ρ'C15–H27	1291	ρ'C15–H27 ρ'C20–H32	1293	ρ'C20–H32	1287	ρ'C15–H27	1286	δ(O–H)
	1275 sh		1280	ρ'C14–H26	1279	ρ'C14–H26 ρ'C20–H32	1278	δ(O11–H45)	1271	τCO4–H38 τO47–H38	1275	δ(O–H)
1268 sh	1272 w		1265	δ(O11–H45) ρCH_2(C23)	1263	δ(O11–H45) wagCH_2(C23)	1273	δ(O11–H45) δ(O7–H41)	1259	ρCH_2(C23)	1266	ρCH_2
1258 w,br	1258 m		1255	δ(O9–H43)	1254	δ(O8–H42)	1255	δ(O4–H38)	1255	δ(O7–H41)	1258	ρCH_2
1241 w	1241 m		1249	δ(O6–H40) δ(O4–H38)	1251	δ(O7–H41)	1248	ρCH_2(C23)			1237	ρC–H
1241 w	1241 m		1237	ρCH_2(C23) δ(O11–H45)	1239	ρCH_2(C23)	1239	ρ'C18–H30 δ(O6–H40)				
	1234 sh		1235	ρ'C18–H30	1237	ρ'C18–H30 δ(O6–H40)	1238	δ(O9–H43)	1237	ρ'C16–H28		
	1230 sh								1231	ρ'C19–H31	1230	ρC–H
1222 sh			1225	δ(O5–H39)	1224	δ(O5–H39)	1219	δ(O11–H45)	1223	ρCH_2(C22)	1225	δ(O–H)
1212 w	1219 sh				1211	ρCH_2(C22) δ(O10–H44)	1212	ρCH_2(C22)			1221	δ(O–H)
	1209 m		1210	ρCH_2(C22)			1199	ρ'C16–H28				
	1209 m				1194	ρ'C16–H28	1194	ρ'C17–H29 δ(O5–H39)	1192	ρ'C17–H29		
	1188 vw		1187	ρ'C16–H28					1186	τCO4–H38 τO47–H38		
1175 sh			1182	ρ'C17–H29 ρ'C19–H31	1180	ρ'C17–H29					1171	βR_1($A6_1$)
1150 m	1149 m										1167	βR_1($A6_1$)
1131 m	1134 sh		1132	ν(C13–O3) ν(C13–C15)	1131	ν(C13–C15)	1132	ν(C17–O7)	1135	ν(C14–O4) βR_1($A6_1$)	1135	βR_1($A6_2$)
	1128 sh		1128	ν(C14–C16)	1128	ν(C15–C17) ν(C12–C14)	1126	ν(C17–O7)	1129	βR_1($A6_2$)	1132	βR_1($A6_2$)
	1118 vs		1123	ν(C16–O6)	1120	ν(C18–O8)	1122	ν(C13–C15)	1124	ν(C15–C17)	1127	βR_1($A6_2$)
	1118 vs		1118	ν(C15–C17)	1115	ν(C17–O7)	1115	ν(C18–O8) ν(C20–C22)	1117	τCO4–H38 τO47–H38	1119	βR_1($A6_2$)
1100 m	1101 s		1112	ν(C17–O7)	1110	ν(C14–C16)	1109	ν(C16–O6)	1106	ν(C12–O2)	1110	ν(C–C)
1100 m	1101 s		1110	ν(C12–O2)	1107	ν(C13–O3)	1102	ν(C15–O5)	1101	τO4–H38 δ(O1C13O3)	1103	ν(C–O)
	1098 sh				1100	ν(C18–O8) ν(C16–O6)	1101	ν(C16–O6)	1096	τR_1 ($A6_1$)	1098	τR_1 ($A6_1$)

(*continued on next page*)

Table 4 (*continued*)

Experimental[a]		Ref[c]	Anhydrous[a]						Dihydrated[a]			
IR	Raman	IR	αα-Trehalose		αβ-Trehalose		ββ-Trehalose		αα-Trehalose		Dimer	
Solid	Solid	Solid	SQM[b]	Assig	SQM[b]	Assig	SQM[b]	Assig	SQM[b]	Assig	Calc.	Assig
	1094 sh		1093	ν(C19–O9)	1092	ν(C19–O9)			1090	ν(C19–O9) ν(C17–O7)	1093	ν(C–O)
1084 m	1086 sh		1088	ν(C18–O8)			1089	ν(C19–O9)	1087	τCO4–H38 τO47–H38	1080	ν(C–O)
	1079 s		1080	ν(C19–C21)	1081	ν(C17–O7) ν(C19–C21)			1081	ν(C18–C20)	1073	ν(C–O)
	1079 s		1071	ν(C14–O4)			1069	ν(C21–C23) τwCH$_2$(C23) δ(C23C21O3)	1074	ν(C19–C21) ν(C21–C23)	1071	ν(C–O)
1062 m	1059 vs		1067	ν(C15–O5)	1067	ν(C15–O5)	1064	ν(C14–O4) ν(C16–O6) ν(C12–O2)			1068	ν(C–O)
1062 m	1059 vs		1063	ν(C18–C20) ν(C20–C22)	1062	ν(C14–O4) ν(C12–O2)	1057	ν(C18–C20)	1063	τR$_1$ (A6$_2$)	1063	ν(C–O)
1055 sh					1056	ν(C22–O10) ν(C18–C20)	1052	ν(C15–O5)			1057	τR$_1$ (A6$_2$)
	1052 sh		1049	ν(C22–O10)	1047	ν(C22–O10)	1046	ν(C22–O10)			1052	τwCH$_2$
	1048 sh		1041	ν(C22–O10)	1040	ν(C22–O10) ν(C23–O11)	1042	ν(C23–O11)	1041	ν(C12–O2)	1047	τwCH$_2$
1032 s									1036	ν(C23–O11) ν(C22–O10)		
1032 s			1032	ν(C23–O11)			1032	ρC15–H27	1031	ν(C13–O3)	1031	ν(C–O)
	1026 w		1025	ν(C19–C21)	1029	ν(C23–O11) ν(C19–C21)			1021	ν(C15–O5)	1028	ν(C–O)
1016 m	1016 w		1009	ν(C12–O1)	1014	ν(C12–O1)					1015	ν(C–O)
998 vs	999 w	**998**	1004	τwCH$_2$(C23)	1005	ν(C21–O3)	1000	ν(C13–O3)	999	ν(C13–O3)	1009	τwCH$_2$
998 vs		**998**							993	ν(C20–O2) τwCH$_2$(C23)	998	ν(C–O)
998 vs		**998**	988	ν(C20–O2)	987	ρC15–H27	987	ν(C21–C23)	991	ν(C20–O2) ν(C18–O8) ν(C16–C18)	987	τO–H
	980 sh		975	ν(C16–C18)							978	τO–H
	965 sh		973	ν(C17–C19)	974	ν(C17–C19)	973	ν(C16–C18)	974	ν(C17–C19)	960	ν(C–C)
957 w	955 w	**956**			966	ν(C16–C18)			967	ν(C13–O1)	955	ν(C–C)
948 sh			949	ν(C13–O1)			943	ν(C17–C19)			941	ν(C–C)
	926 m				933	ν(C12–O1)	930	ν(C13–O1) ν(C12–O1)	923	ν(C13–C15) ν(C12–O1) ν(C12–C14)	939	τO–H
	917 sh								913	τCO4–H38 τO47–H38	918	ν(C–O)
911 w	910 s		908	ν(C12–O1) ν(C12–C14)	905	ν(C13–O1)	901	ν(C19–C21)	911	τCO4–H38 τO47–H38	909	ν(C–O)

881 sh		881	δ(C12O1C13)	884	ν(C18–C20)	890	ν(C19–C21)	892	τCO4–H38 δ(O4H38O47)	879	τO–H
864 m,br						870	ν(C18–O8)	863	τO11–H45 τO4–H38	856	τO–H
852 m	850 sh			859	ν(C18–O8) ν(C16–C18)	851	ρC15–H27			855	τO–H
842 m	839 vs									847	τO–H
		816	ν(C21–O3)	820	τwCH$_2$(C23) βR$_1$(A6$_1$)	818	βR$_1$(A6$_2$) βR$_1$(A6$_1$)			833	τwCH$_2$
804	804 w	804	δ(O1C13O3) δ(C14C12O1) δ (O1C13C15)	812	ν(C21–O3) τwCH$_2$(C23)			807	δ(O1C13O3) δ(O1C13C15)	810	δ(OCO) δ(OCC)
	796 sh	798	ν(C20–O2) τwCH$_2$(C22)			798	ν(C21–O3)	791	τwCH$_2$(C22)	806	τwCH$_2$
				777	ν(C20–O2) τwCH$_2$(C22)	780	ν(C20–O2) τwCH$_2$(C22)	785	ν(C21–O3) τwCH$_2$(C23)	779	ρH$_2$O
				744	ν(C20–O2)	757	ν(C20–O2)			747	wagH$_2$O
732 w,br	731 w					724	δ(O1C13O3)	728	τCO4–H38 τO47–H38	728	τO–H
711 sh	709 sh	711	βR$_1$(A6$_1$) βR$_1$(A6$_2$)					716	τCO4–H38 τO47–H38	719	τO–H
698 w	697 m			690	ν(C14–C16)	689	ν(C15–C17)	699	τCO4–H38 τO47–H38	706	βR$_1$(A6$_2$)
						686	ν(C14–C16)			682	ρH$_2$O
		673	δ(O2C12O1)	678	τR$_2$ (A6$_1$)	672	ν(C15–C17)	674	δ(O11H45O46)	679	ρH$_2$O
669 w,br	669 w			667	δ(O2C12O1)	668	δ(O1C13O3) δ(O2C12O1) δ(C17C19O9)			663	ρH$_2$O
669 w,br	669 w							656	τCO4–H38 τO47–H38	661	ρH$_2$O
645 w,br	629 sh	631	ρC15–H27	624	ρC15–H27					643	ρH$_2$O
614 w,br	617 w					616	δ(C14C12O1)	608	τCO4–H38 τO47–H38	617	τO–H
	601 m	600	δ(O6C16C18) δ (C20C22O10)							601	βR$_1$(A6$_1$)
	601 m	594	δ(C21C23O11)	593	δ(C21C23O11)			588	δ(C21C23O11)	598	δ(CCO)
583 w	576 w							574	δ(O1C13O3) δ(O5C15C17)	577	τO–H
560 sh		569	δ(O5C15C17) δ(O1C13O3)	563	δ(O1C13O3)					571	τO–H
	550 sh	552	δ(O8C18C16)					547	τCO4–H38 τO47–H38	552	τO–H

(*continued on next page*)

Table 4 (*continued*)

Experimental[a]		Ref[c]	Anhydrous[a]						Dihydrated[a]			
IR	Raman	IR	αα-Trehalose		αβ-Trehalose		ββ-Trehalose		αα-Trehalose		Dimer	
Solid	Solid	Solid	SQM[b]	Assig	SQM[b]	Assig	SQM[b]	Assig	SQM[b]	Assig	Calc.	Assig
	540 vs						542	δ(O1C13O3)			548	$\tau R_3(A6_1)$
538 w			532	δ(C17C19O9)	537	δ(C17C19O9) δ(C21C19O9)			534	τCO4–H38 τO47–H38	538	τwH_2O
518 w	520 s		524	τR_1 ($A6_1$)					522	τCO4–H38 δ(O1C13O3)	522	τwH_2O
501 sh	506 sh				504	ρC15–H27	494	ρC15–H27	496	$\tau R_3(A6_1)$ δ(O6C16C18) δ (O8C18C20)	504	δ(OCC)
					476	τO6–H40 τO4–H38	475	δ(C20C22O10)			498	τO–H
					473	δ(C20C22O10) δ(C20C22O10)	473	τO6–H40	469	τO10–H44	465	τO–H
							459	δ(C21C23O11) $\beta R_2(A6_2)$ τR_1 ($A6_2$)	456	τO5–H39	459	τO–H
445 w	448 s		450	τO4–H38	445	τO5–H39	448	τO5–H39 τO7–H41	451	ρH_2O(W1) δ(O4H38O47)	443	τO–H
442 sh	440 sh		441	τO5–H39	440	τO8–H42	437	τO8–H42			442	$\beta R_2(A6_2)$
430 w	429 sh		433	τO10–H44							433	δ(CCO)
			428	$\beta R_2(A6_2)$	425	τO5–H39			428	δ(C23C21O3)	430	$\beta R_2(A6_2)$
			425	τO5–H39					424	τO8–H42 δ(C23C21C19)	428	δ(CCO)
	423 sh				419	$\beta R_2(A6_2)$			423	$\beta R_2(A6_2)$	424	$\beta R_2(A6_2)$
			415	$\beta R_2(A6_2)$	414	δ(O4C14C16)	415	δ(O4C14C16) ν(C12–C14)	413	τO6–H40 βR_2 ($A6_1$)	415	βR_2 ($A6_1$)
410 w	407 vs						409	τO7–H41	407	τCO4–H38 τO47–H38	406	βR_2 ($A6_1$)
	400 sh		399	$\beta R_3(A6_1)$					405	τCO4–H38 τO47–H38	404	βR_2 ($A6_1$)
			396	$\beta R_3(A6_2)$	397	$\beta R_3(A6_2)$	392	τO10–H44	398	$\beta R_3(A6_2)$	400	βR_2 ($A6_2$)
	393 sh		394	τO10–H44	388	τO10–H44	389	τO9–H43				
			381	τO9–H43	380	τO10–H44 τO4–H38	382	τO4–H38				
	375 sh		380	τO8–H42 τO6–H40	377	τO9–H43			378	τO9–H43 τO7–H41	381	$\beta R_3(A6_1)$
	370 s		366	δ(O6C16C14)			369	$\beta R_3(A6_2)$	370	δ(C15C17O7)	370	δ(CCC)
	365 sh		364	δ(C15C17O7)	362	δ(C15C17O7)	366	$\beta R_3(A6_1)$			363	$\beta R_3(A6_1)$
	360 sh				361	$\beta R_3(A6_1)$					358	τCO–H
	354 sh		356	τO7–H41	352	τO7–H41	350	τO5–H39	354	τCO4–H38	352	τwH_2O
	342 w						340	δ(O5C15C17)			340	τwH_2O
			334	τO10–H44			333	δ(O4C14C16)	334	τCO4–H38	336	τCO–H

							τO10–H44		
317 m			329	τO10–H44			322	τCO4–H38 τO47–H38	320 τCO–H
	307	δ(O8C18C20)					308	τO11–H45 ρH_2O(W1)	313 δ(OCC)
300 m	304	δ(C21C19O9)	306	δ(O6C16C14)	306	δ(O8C18C20)	307	τO11–H45 τCO4–H38	307 ρH_2O
293 sh			298	δ(O8C18C20) δ(O2C20C22)	293	δ(C21C19O9) δ (C23C21O3)	288	wagH_2O(W1) ν(O46–H45)	297 δ(OCC)
281 sh					282	δ(C21C19O9)	284	δ(O4C14C12)	284 δ(CCO)
			276	δ(O8C18C16)			276	wagH_2O(W1)	278 wagH_2O
269 sh					271	δ(O6C16C14)	271	τO47–H38 τCO4–H38	273 δ(OCC)
	258	δ(O5C15C13)							258 δ(OCC)
256 sh	254	δ(O5C15C17)	253	δ(O5C15C17)			255	δ(O5C15C17) δ(O5C15C13)	250 δ(OCC)
249 w	247	δ(O5C15C17) δ (O4C14C16)	250	δ(O6C16C18)	250	δ(O6C16C18)	248	τO46–H45	247 δ(OCC)
	240	δ(C19C17O7)	238	δ(C19C17O7)	241	δ(O5C15C13) δ(C19C17O7)	237	τO47–H38 τCO4–H38	237 δ(OCC)
235 sh	231	τR_1 ($A6_2$)					235	τO11–H45	230 τR_1 ($A6_1$)
223 sh			232	δ(O5C15C13) τO11–H45	229	ρC15–H27	230	τR_1 ($A6_1$) δ (C19C17O7)	229 τR_1 ($A6_1$)
216 m	216	δ(O4C14C12)			215	δ(O4C14C12)	214	τO46–H45 τO11–H45	221 δ(CCC)
209 sh			211	δ(O4C14C12)			212	τR_2 ($A6_1$) δ (C12O1C13)	206 τR_2 ($A6_1$)
202 w	194	δ(O2C20C22)	193	δ(O5C15C13)	195	δ(O2C20C22)			197 ν(O–H)
189 sh	184	βR_2 ($A6_1$)	180	τO11–H45 δ(C23C21O3)	187	τO11–H45	182	ν(O47–H38)	185 ν(O–H)
	178	τO11–H45	170	δ(C23C21C19)			178	τO4–H38	183 ν(O–H)
160 vw					161	δ(C18C20C22) βR_2 ($A6_1$)	163	τO11–H45	164 ν(O–H)
160 vw	157	δ(C18C20C22)	151	δ(C18C20C22)	151	δ(C23C21C19)			157 ν(O–H)
			132	τR_3($A6_1$)	135	τR_3($A6_1$) τR_1 ($A6_1$)	144	τwC12–O1 τwC13–O1	138 τR_3($A6_1$)
	126	τR_2 ($A6_2$)	122	τR_2 ($A6_2$) τR_1 ($A6_2$)	126	τR_2 ($A6_2$)	127	τCO4–H38 ττO47–H38	122 τR_3($A6_2$)
	118	τwC20–C22 τR_3($A6_1$)			113	τR_3 ($A6_2$)	118	τR_2 ($A6_2$)	114 τR_3($A6_2$)
110 vw,br	111	τR_3 ($A6_2$)	110	τR_3 ($A6_2$)	100	τwC20–C22	110	τwC21–C23	112 τR_3($A6_2$)

(*continued on next page*)

Table 4 (*continued*)

Experimental[a]		Ref[c]	Anhydrous[a]						Dihydrated[a]			
IR	Raman	IR	αα-Trehalose		αβ-Trehalose		ββ-Trehalose		αα-Trehalose		Dimer	
Solid	Solid	Solid	SQM[b]	Assig	SQM[b]	Assig	SQM[b]	Assig	SQM[b]	Assig	Calc.	Assig
										τR_3 ($A6_2$)		
			97	τwC21–C23	96	τwC20–C22					97	τwC–C
		80.1	86	τwC21–C23	86	τwC21–C23	88	τwC21–C23	90	τO47–H38 τCO4–H38	90	τwC–C
		72.4					68	τR_3($A6_1$) τR_2 ($A6_1$)	74	τCO4–H38τO47–H38	74	τwC–C
			61	τR_2 ($A6_1$)	64	τR_3($A6_1$) τR_3 ($A6_2$)	67	τR_2 ($A6_1$)	61	τOC4–H38 τO47–H38	65	τOC–H
	54 vw,br	**56.6**	57	δ(C23C21C19)	58	τR_2 ($A6_1$)					59	τOC–H
		49.3							52	τO47–H38 τCO4–H38	55	τOC–H
		47.4							44	τO4–H38	47	τO–H
		43.1							43	τO47–H38	44	τOC–H
		38.1	39	τR_2 ($A6_1$) τR_2 ($A6_2$)	40	δ(C12O1C13) δ(C14C12O1) δ (O1C13C15)	41	δ(C12O1C13) δ(O1C13C15)			38	τwC–O
							29	τwC12–O1	30	τCO4–H38 τO47–H38	32	δ(OCC)
			23	τwC12–O1					28	τCO4–H38 τO47–H38	27	δ(OCC)
	18 sh		19	τwC13–O1	22	τwC13–O1	23	τwC13–O1	21	τCO47–H38 τO4–H38	23	τwC–O
	13 sh				16	τwC12–O1					15	τwC–O

Abbreviations: ν, stretching; β, deformation in the plane; γ, deformation out of plane; wag, wagging; τ, torsion; β_R, deformation ring τ_R, torsion ring; ρ, rocking; τw, twisting; δ, deformation; a, antisymmetric; s, symmetric; ($_1$), glucopyranose Ring1; ($_2$), glucopyranose Ring2. [a]This work, [b]From scaled quantum mechanics force field Bold letter, values taken from Ref[c] (Takahashi et al., 2006).

Table 5 Comparison of scaled internal force constants for the trehalose species in the gas phase with those corresponding to maltose and lactose in the same phase.

B3LYP/6-31G*											
Force constant	Trehalose[a]				Maltose[b]				Lactose[c]		
	Anhydrous			Dihydrated	Anhydrous		Monohydrated		Anhydrous		Monohydrated
	αα-	αβ-	ββ-	αα-	α-	β-	α-	β-	α-	β-	α-
$f(\nu O–H)_{H2O}$				6.88			7.25	7.05			6.96
$f(\nu O–H)$	7.14	7.16	7.11	6.94	7.09	7.04	7.00	6.96	7.12	7.10	7.00
$f(\nu CH_2)$	4.73	4.75	4.75	4.81	4.81	4.79	4.82	4.75	4.73	4.73	4.82
$f(\nu C–H)$	4.71	4.71	4.73	4.71	4.70	4.73	4.74	4.78	4.64	4.59	4.65
$f(\nu C–O)_C$	4.42	4.41	4.38	4.54	4.73	4.78	4.45	4.75	4.67	4.68	4.65
$f(\nu C–O)_H$	5.04	5.03	5.05	5.07	5.02	4.94	5.10	4.96	5.02	5.11	3.82
$f(\nu C–C)$	4.00	4.01	3.97	4.14	3.88	3.86	3.90	3.96	3.91	3.91	3.91
$f(\delta C–O–C)$	1.18	1.14	1.19	2.31	2.50	2.64	2.27	2.78	1.88	1.89	1.92
$f(\delta C–O–H)$	0.80	0.80	0.80	1.01	0.76	0.78	0.82	0.95	0.74	0.74	0.83
$f(\delta H–C–H)$	0.81	0.81	0.81	0.82	0.85	0.80	0.80	0.90	0.82	0.82	0.81

Units are mdyn $Å^{-1}$ for stretching and mdyn Å rad^{-2} for angle deformations.
[a] This work,
[b] From Ref. Iramain et al. (2016),
[c] From Ref. Márquez et al. (2015a,b).

the C–C stretching modes are assigned to the bands between 1171 and 668 cm^{-1}, as predicted by calculations, in this species, these modes are predicted and assigned in the 1131–672 cm^{-1} region, as can be seen in Table 4. The remaining vibration modes for the anhydrous, dihydrated and dimeric species are indicated in Table 4 and they correspond to the deformation and torsions of both glucopyranose rings and to the OCO, CCC, CCO and OCC deformation modes which are predicted in the lower wavenumbers region.

4.7. Force field

For the three anhydrous species of trehalose and their dihydrated form the force constants were computed using the SQMFF methodology (Rauhut and Pulay, 1995a) with the Molvib program (Sundius, 2002). The results in the gas phase at the B3LYP/6-31G* level of theory are presented in Table 5 together with those values reported for the maltose and lactose species (Márquez et al., 2015a,b; Iramain et al., 2016) at the same level of theory. Comparing first the values for the anhydrous species, we observed that the three species show practically the same values and there are no significant changes among them, however, when these values are compared with those corresponding to the dihydrated species all the values slightly increase for this species in relation to the anhydrous species with exception of the $f(\nu O–H)$ force constant whose value decrease for the dihydrated species. This observation is probably related with the higher quantity of intra-molecular interactions observed for this species using NBO and AIM studies (Tables S5–S7). On the other hand, the anhydrous species of maltose and lactose show higher values in the $f(\delta C–O–C)$ force constants related to the glycosidic bonds, between 2.78 and 1.88 mdyn $Å^{-1}$ as compared with those corresponding to trehalose (1.19–1.14 mdyn $Å^{-1}$) while the hydrated species of trehalose present a force constant value (2.31 mdyn $Å^{-1}$) between those corresponding to maltose (2.78–2.27 mdyn $Å^{-1}$) and lactose (1.92 mdyn $Å^{-1}$). Here, the $f(\delta C–O–C)$ force constants related to the glycosidic bonds evidence clearly the different characteristics in the three sugars: maltose > trehalose > lactose but these values are not justified because maltose and lactose are reducing sugars while trehalose is a non-reducing sugar. Hence, the behavior electrophilic of trehalose could also be related to their $f(\nu O–H)_{H2O}$ force constant because the value for the dihydrated trehalose is 6.88 mdyn $Å^{-1}$ while for monohydrated lactose is 6.96 mdyn $Å^{-1}$ and for monohydrated maltose 7.25–7.05 mdyn $Å^{-1}$. Here, the low $f(\nu O–H)_{H2O}$ force constant value for trehalose are strongly related to the lowest BO values observed in particular for the O–H bonds corresponding to the water molecules. This way, the following relation is observed in the $f(\nu O–H)_{H2O}$ force constants: trehalose < lactose < maltose showing a low $f(\nu O–H)_{H2O}$ force constant value for trehalose which could justify: (i) the very fragile character from the trehalose–water system to the temperature and concentration changes, as experimentally was reported by Branca et al. (1999) from viscosity and Raman scattering studies, (ii) why the presence of the disaccharides inhibits the protein dynamical transition (Magazù et al., 1998) from studies of the influence of hydrogen bond connectivity on transport properties for the same trehalose–water system, (iii) the non-reducing property of this sugar and, (iv) the ability of trehalose to form H bonds and, this way, to stabilize the membranes, as reported by Crowe and Crowe (1984).

5. Conclusions

In this work, the dihydrated trehalose form was completely characterized using the FTIR and Raman spectroscopy combined with DFT calculations. The structures of three anhydrous species of trehalose, the dihydrated form and their dimer were theoretically determined in gas phase and aqueous solution using the hybrid B3LYP/6-31G* method. In aqueous solution, the calculations were computed with the PCM and SD models in order to predict the solvation energies. Both

NBO and AIM studies reveal high stability for the dihydrated species in solution that could probably explain the formation of several intermolecular hydrogen bonds where are involved every hydroxyl group in the system generating, this way, higher ''rigidity'' in trehalose and a lower volume expansion and solvation energy for trehalose in solution, in relation to maltose and sucrose. Besides, the low $f(vO–H)_{H2O}$ force constant value for trehalose could justify the very fragile character from the trehalose–water system to the temperature and concentration changes among other properties. In addition, the studies using the frontier orbitals show the high gap values observed for the anhydrous and dihydrated species of trehalose which probably justify why it is a nonreducing disaccharide of glucose while the similar lower gap values predicted for maltose and lactose probably justify that these carbohydrates are reducing sugars. Finally, the complete vibrational assignments for the anhydrous and dihydrated form of trehalose were performed using the scaled mechanical force fields.

Acknowledgements

This work was subsidized with grants from CIUNT Project 26/D207 (Consejo de Investigaciones, Universidad Nacional de Tucumán). The authors thank Prof. Tom Sundius for his permission to use MOLVIB.

Appendix A. Supplementary data

Supplementary data associated with this article can be found, in the online version, at http://dx.doi.org/10.1016/j.jksus.2017.01.009.

References

Ballone, P., Marchi, M., Branca, C., Magazù, S., 2000. Structural and vibrational properties of trehalose: a density functional study. J. Phys. Chem. B 104, 6313–6317.

Becke, A.D., 1993. Density functional thermochemistry. III. The role of exact exchange. J. Chem. Phys. 98, 5648–5652.

Belton, P.S., Gil, A.M., 1994. IR and Raman spectroscopic studies of the interaction of Trehalose with Hen Egg white Lysozyme. Biopolymers 34, 957–961.

Besler, B.H., Merz, K.M., Kollman, P.A.J., 1990. Atomic charges derived from demiempirical methods. Comput. Chem. 11, 431–439.

Biegler-Köning, F., Schönbohm, J., Bayles, D.J., 2001. AIM2000; a program to analyze and visualize atoms in molecules. Comput. Chem. 22, 545–549.

Bonanno, G., Noto, R., Fornili, S.L., 1998. Water interaction with a, a-trehalose: molecular dynamics simulation, J. Chem. Soc. Faraday Trans. 94, 2755–2762.

Branca, C., Magazù, S., Maisano, G., Migliardo, P., Villari, V., Sokolov, A.P., 1999. The fragile character and structure-breaker role of α, α-trehalose: viscosity and Raman scattering findings. J. Phys. Condens. Matter 11, 3823–3832.

Branca, C., Magazù, S., Maisano, G., Migliardo, F., 2001. Vibrational and relaxational contributions in disaccharide/H_2O glass formers. Phys Rev B 64, 224204–224208.

Branca, C., Magazù, S., Migliardo, F., Migliardo, P., 2002. Destructuring effect of trehalose on the tetrahedral network of water: a Raman and neutron diffraction comparison. Phys. A 304, 314–318.

Brédas, J.-L., 2014. Mind the gap! Mater. Horizons 1, 17–19.

Brizuela, A.B., Bichara, L.C., Romano, E., Yurquina, A., Locatelli, S., Brandán, S.A., 2012a. A complete characterization of the vibrational spectra of sucrose. Carbohydr. Res. 361, 212–218.

Brizuela, A.B., Romano, E., Yurquina, A., Locatelli, S., Brandán, S. A., 2012b. Experimental and theoretical vibrational investigation on the saccharinate ion in aqueous solution. Spectrochim. Acta Part A 95, 399–406.

Brizuela, A.B., Castillo, M.V., Raschi, A.B., Davies, L., Romano, E., Brandán, S.A., 2014. A complete assignment of the vibrational spectra of sucrose in aqueous medium based on the SQM methodology and SCRF calculations. Carbohyd. Res. 388, 112–124.

Brown, G.M., Rohrer, D.C., Berking, B., Beevers, C.A., Gould, R.O., Simpson, R., 1972. The crystal structure of,-trehalose dihydrate from three independent X-ray determinations. Acta Cryst. B28, 3145–3158.

Calabrò, E., Magazù, S., 2012. Electromagnetic fields effects on the secondary structure of lysozyme and bioprotective effectiveness of Trehalose. Adv. Phys. Chem., 6 Article ID 970369.

Cataldo, P.G., Castillo, M.V., Brandán, S.A., 2014. Quantum mechanical modeling of fluoromethylated-pyrrol derivatives a study on their reactivities, structures and vibrational propertiesJ. Phys. Chem. Biophys. 4 (1), 2–9.

Connolly, B., Patapoff, T.W., Wang, Y.J., Moore, J.M., Kamerzell, T. J., 2010. Vibrational spectroscopy and chemometrics to characterize and quantitate trehalose crystallization. Anal. Biochem. 399, 48–57.

Crowe, J.H. Crowe, L.M., 1984. Preservation of Membranes in Anhydrobiotic Organisms: The Role of Trehalose, 702–703.

Frisch, M.J., Trucks, G.W., Schlegel, H.B., Scuseria, G.E., Robb, M. A., Cheeseman, J.R., Scalmani, G., Barone, V., Mennucci, B., Petersson, G.A., Nakatsuji, H., Caricato, M., Li, X., Hratchian, H. P., Izmaylov, A.F., Bloino, J., Zheng, G., Sonnenberg, J.L., Hada, M., Ehara, M., Toyota, K., Fukuda, R., Hasegawa, J., Ishida, M., Nakajima, T., Honda, Y., Kitao, O., Nakai, H., Vreven, T., Montgomery, J.A., Jr., Peralta, J.E., Ogliaro, F., Bearpark, M., Heyd, J.J., Brothers, E., Kudin, K.N., Staroverov, V.N., Kobayashi, R., Normand, J., Raghavachari, K., Rendell, A., Burant, J.C., Iyengar, S.S., Tomasi, J., Cossi, M., Rega, N., Millam, J.M., Klene, M., Knox, J.E., Cross, J.B., Bakken, V., Adamo, C., Jaramillo, J., Gomperts, R., Stratmann, R.E., Yazyev, O., Austin, A.J., Cammi, R., Pomelli, C., Ochterski, J.W., Martin, R.L., Morokuma, K., Zakrzewski, V.G., Voth, G.A., Salvador, P., Dannenberg, J.J., Dapprich, S., Daniels, A.D., Farkas, Ö., Foresman, J.B., Ortiz, J. V., Cioslowski, J., Fox, D.J., 2009. Gaussian Inc, Wallingford CT.

Glendening, E.D., Badenhoop, J.K., Reed, A.D., Carpenter, J.E., Weinhold, F., 1996. NBO3.1; Theoretical Chemistry Institute. University of Wisconsin, Madison, WI.

Govindarajan, R., Chatterjee, K., Gatlin, L., Suryanarayanan, R., Shalaev, E.Y.J., 2006. Impact of freeze-drying on ionization of sulfonephthalein probe molecules in trehalose-citrate systems. Pharm. Sci. 95 (7), 1498–1509.

Iramain, M.A., Davies, L., Brandán, S.A., 2016. FTIR, HATR and FT-Raman studies on the anhydrous and monohydrate species of maltose in aqueous solution. Carbohyd. Res. 428, 41–56.

Kawashima, H., Goto, H., 2011. Preparation and properties of polyaniline in the presence of Trehalose. Soft Nanosci. Lett. 1, 71–75.

Lee, C., Yang, W., Parr, R.G., 1988. Development of the Colle-Salvetti correlation-energy formula into a functional of the electron density. Phys. Rev. 41, 785–789.

Magazù, S., Maisano, G., Middendorf, H.D., Migliardo, F., Mussolino, A.M., Villari, V., 1998. α,α-Trehalose-water solutions. II Influence of hydrogen bond connectivity on transport properties. J. Phys. Chem. B 102, 2060–2063.

Magazù, S., Maisano, G., Migliardo, P., Villari, V., 1999. Experimental simulation of macromolecules in trehalose aqueous solutions: a photon correlation spectroscopy study. J. Chem. Phys. 111 (19), 9086–9092.

Magazù, S., Migliardo, F., Telling, M.T.F., 2007. Study of the dynamical properties of water in disaccharide Solutions. Eur. Biophys. J. 36, 163–171.

Magazù, S., Calabrò, E., Campo, S., 2010. FTIR spectroscopy studies on the bioprotective effectiveness of trehalose on human hemoglobin aqueous solutions under 50 Hz electromagnetic field exposure. J. Phys. Chem. B 114, 12144–12149.

Magazù, S., Migliardo, F., Benedetto, A., 2010. Mean square displacements from elastic incoherent neutron scattering evaluated by spectrometers working with different energy resolution on dry and hydrated (H_2O and D_2O) Lysozyme. J. Phys. Chem. B 114, 9268–9274.

Magazù, S., Migliardo, F., Benedetto, A., Mondelli, C., Gonzalez, M. A., 2011. Thermal behaviour of hydrated lysozyme in the presence of sucrose and trehalose by EINS. J. Non-Cryst. Solids 357, 664–670.

Marenich, A.V., Cramer, C.J., Truhlar, D.G., 2009. Universal solvation model based on solute electron density and a continuum model of the solvent defined by the bulk dielectric constant and atomic surface tensions. J. Phys. Chem. B 113, 6378–6396.

Márquez, M.B., Brandán, S.A., 2014. A structural and vibrational investigation on the antiviral deoxyribonucleoside thymidine agent in gas and aqueous solution phases. Int. J. Quantum Chem. 114 (3), 209–221.

Márquez, M.J., Brizuela, A.B., Davies, L., Brandán, S.A., 2015. Spectroscopic and structural studies on lactose species in aqueous solution combining the HATR and Raman spectra with SCRF calculations. Carbohyd. Res. 407, 34–41.

Márquez, M.J., Márquez, M.B., Cataldo, P.G., Brandán, S.A., 2015. A comparative study on the structural and vibrational properties of two potential antimicrobial and anticancer cyanopyridine derivatives OJSTA 4, 1–19.

Miertus, S., Scrocco, E., Tomasi, 1998. Electrostatic interaction of a solute with a continuum. J. Chem. Phys. 55, 1117.

Nielsen, A.B., Holder A.J., 2008. Gauss View 5.0, User's Reference, GAUSSIAN Inc., Pittsburgh, PA.

Olsson, Christoffer, Jansson, Helén, Swenson, Jan, 2016. The Role of Trehalose for the Stabilization of Proteins. J. Phys. Chem. B 120, 4723–4731.

Pagnotta, S.E., Ricci, M.A., Bruni, F., McLain, S., Magazù, S., 2008. Water structure around trehalose. Chem. Phys. 345, 159–163.

Parr, R.G., Pearson, R.G., 1983. Absolute hardness: companion parameter to absolute electronegativity. J. Am. Chem. Soc. 105, 7512–7516.

Rauhut, G., Pulay, P., 1995a. Transferable scaling factors for density functional derived vibrational force fields. J. Phys. Chem. 99, 3093–3099.

Rauhut, G., Pulay, P., 1995b. Transferable scaling factors for density functional derived vibrational force fields. J. Phys. Chem. 99, 14572.

Romani, D., Brandán, S.A., 2015a. Structural and spectroscopic studies of two 1,3-benzothiazole tautomers with potential antimicrobial activity in different media. Prediction of their reactivities Comput. Theor. Chem. 1061, 89–99.

Romani, D., Brandán, S.A., Márquez, M.J., Márquez, M.B., 2015b. Structural, topological and vibrational properties of an isothiazole derivatives series with antiviral activities. J. Mol. Struct. 1100, 279–289.

Schebor, C., Mazzobre, M.F., Buera, M.P., 2010. Glass transition and time-dependent crystallization behavior of dehydration bioprotectant sugars. Carbohyd. Res. 345, 303–308.

Shibata, M., Nagashima, S., 2016. Trehalose-incorporated organic–inorganic hybrid nanocomposites produced by thiol-ene photopolymerization. Polym. J. 48, 111–116.

Siddhanta, S., Barman, I., Narayana, C., 2015. Illuminating trehalose mediated inhibition of protein aggregation through lysozyme-silver nanoparticle interaction. Soft Matter. 11 (37), 7241–7249.

Sundius, T., 2002. Scaling of ab-initio force fields by MOLVIB. Vib. Spectrosc. 29, 89–95.

Taga, T., Senma, M., Osaki, K., 1972. The crystal and molecular structure of trehalose dihydrate. Acta Cryst. B28, 3258–3263.

Takahashi, M., Kawazoe, Y., Ishikawa, Y., Ito, H., 2006. Low-frequency vibrations of crystalline a, a-trehalose dehydrate. Chem. Phys. Lett. 429, 371–377.

Tomasi, J., Persico, M., 1994. Molecular interactions in solution: an overview of methods based on continuous distributions of the solvent. Chem. Rev. 94, 2027.

Ugliengo, P., 1998. MOLDRAW Program. University of Torino, Dipartimento Chimica IFM, Torino, Italy.

Varga, B., Migliardo, F., Takacs, E., Vertessy, B., Magazù, S., Mondelli, C., 2008. Neutron scattering studies on dUTPase complex in the presence of bioprotectant systems. Chem. Phys. 345, 250–258.

Yano, S., Teramoto, N., Miyamoto, R., Nakajima, E., Hashimoto, K., Shibata, M., 2015. Fibroblast cell proliferation on photo-cured trehalose cinnamoyl ester thin films. J. Bioact. Compatible Polym. 30 (1), 87–98.